Toxicology Letters 198 (2010) 324–330

Contents lists available at ScienceDirect

Toxicology Letters

journal homepage: www.elsevier.com/locate/toxlet

In vitro evaluation of SiC nanoparticles impact on A549 pulmonary cells: Cyto-, genotoxicity and oxidative stress

S. Barillet[a], M.-L. Jugan[a], M. Laye[a], Y. Leconte[b], N. Herlin-Boime[b], C. Reynaud[b], M. Carrière[a,*]

[a] *Laboratoire de Structure et Dynamique par Résonance Magnétique, CEA-CNRS UMR3299 SIS2M, IRAMIS, CEA Saclay, bât 639 pce 10, 91191 Gif sur Yvette, France*
[b] *Laboratoire Francis Perrin, CEA-CNRS URA2453, IRAMIS, CEA Saclay, 91191 Gif sur Yvette, France*

ARTICLE INFO

Article history:
Received 7 June 2010
Received in revised form 13 July 2010
Accepted 19 July 2010
Available online 23 July 2010

Keywords:
Silicon carbide
Nanoparticles
Characterization
Toxicity
Oxidative stress

ABSTRACT

Silicon carbide (SiC) is considered a highly biocompatible material, consequently SiC nanoparticles (NPs) have been proposed for potential applications in diverse areas of technology. Since no toxicological data are available for these NPs, the aim of this study was to draw their global toxicological profile on A549 lung epithelial cells, using a battery of classical *in vitro* assays. Five SiC-NPs, with varying diameters and Si/C ratios were used, and we show that these SiC-NPs are internalized in cells where they cause a significant, though limited, cytotoxic effect. Cell redox status is deeply disturbed: SiC-NP exposure cause reactive oxygen species production, glutathione depletion and inactivation of some antioxidant enzymes: glutathione reductase, superoxide dismutase, but not catalase. Finally, the alkaline comet assay shows that SiC-NPs are genotoxic. Taken together, these data prove that SiC-NPs biocompatibility should be revisited.

1. Introduction

Silicon carbide (SiC) has remarkable properties and among them this material is very hard and thermally stable. It possesses particular photoluminescence properties, and a presumed good biocompatibility. For this reason it is largely used for industrial purposes, mainly as micro-sized particles. Several applications using nano-sized SiC particles are emerging, and these materials are considered promising for power electronics, heterogeneous catalysis supports, as ceramics and biomaterials (Melinon et al., 2007). It is thus important to collect information on their toxicity, since their production but also the bad recycling of nanoproducts containing SiC may lead to exposure of workers, populations and ecosystems.

Toxicological information concerning micro- or macroscaled SiC particles is available in the literature, most of them conducted with SiC fibers. *In vivo*, these particles induce damage to the lungs, particularly inflammation (Cullen et al., 1997; Lapin et al., 1991), increased alveolar macrophage number (Vaughan et al., 1993), cell proliferation and hyperplasia of lung and lymph node tissues (Akiyama et al., 2007; Cullen et al., 1997; Lapin et al., 1991), granulomas (Vaughan et al., 1993), lung fibrosis (Akiyama et al., 2007; Lapin et al., 1991), as well as increased cancer incidence (Rodelsperger and Bruckel, 2006). *In vitro*, SiC fibers or particles are reported to be cytotoxic, leading cell membranes disruption (Vaughan et al., 1991). Upon cell exposure to these particles, cellular phenomena associated with malignant transformation (shortened cell generation time, increased DNA synthesis, growth control loss) are reported (Vaughan et al., 1991), together with reactive oxygen species generation (Svensson et al., 1997), antioxidant depletion in lung lining fluid (Brown et al., 2000), and stimulation of cytokine production (Cullen et al., 1997). These particles are also described as genotoxic (Svensson et al., 1997). Conversely, other studies came to the conclusion that SiC exert no harmful effects on tissues, suggesting that they can be considered as inert and thus biocompatible (Bruch et al., 1993a,b).

Although SiC particles are becoming more and more produced at the nano-scale and used in the industry, no comprehensive study describes the toxicological impact of SiC nanoparticles (NPs). The aim of this work was to fill this gap, and to record first information concerning SiC-NPs toxicity. A series of assays was thus conducted on the A549 cell line, derived from a human bronchoalveolar carcinoma. The toxicity of nanoparticles is known to be closely related to their physico-chemical characteristics, and among them the size, shape, specific surface area, surface charge and chemical composition (Lewinski et al., 2008). In order to establish such relationship, we investigated the toxicity of SiC-NPs varying in their diameters (10–60 nm) and Si/C ratios, the latter modulating their surface properties since a high Si/C ratio means the prevalence of Si at the surface of nanoparticles, while a low Si/C ratio means the preva-

* Corresponding author. Tel.: +33 1 69 08 52 35; fax: +33 1 69 08 69 23.
E-mail addresses: Sabrina.barillet@cea.fr (S. Barillet), mary-line.jugan@cea.fr (M.-L. Jugan), mathilde.laye@cea.fr (M. Laye), Yann.leconte@cea.fr (Y. Leconte), nathalie.herlin@cea.fr (N. Herlin-Boime), cecile.reynaud@cea.fr (C. Reynaud), marie.carriere@cea.fr (M. Carrière).

0378-4274/$ – see front matter © 2010 Elsevier Ireland Ltd. All rights reserved.
doi:10.1016/j.toxlet.2010.07.009

lence of C atoms which might be rapidly oxidized as SiO_2 at the surface of nanoparticles. The toxicological behavior of NPs bearing a low Si/C ratio may thus be close to the behavior of carbon-based NPs, while when Si/C ratio is high they may behave as silica-based NPs. After a precise physico-chemical characterization, the potential uptake of NP-SiC in A549 cells was evaluated, together with their cytotoxic and genotoxic potential. Possible underlying mechanisms of toxic action were investigated through the following of several markers of oxidative stress.

To the best of our knowledge, this is the first comprehensive study of NP-SiC toxicity. While these NPs are generally considered biocompatible, we demonstrate that they activate, *in vitro*, several markers of toxicity, and may thus be handled with caution.

2. Materials and methods

2.1. Chemicals and nanopowders

Chemicals and cell culture media were obtained from Sigma–Aldrich. SiC nanopowders were synthesized by laser pyrolysis of gaseous precursors: silane (SiH_4) and acetylene (C_2H_2) (Bouclé et al., 2005). During the synthesis, by controlling the ratio of Si and C gaseous precursors, reactant flow rates and the laser power, SiC nanoparticles with controlled structure can be produced, *e.g.* controlled size and Si/C ratio (Herlin-Boime et al., 2004). Nanoparticles with diameters ranging from 13 nm to 68 nm and Si/C ratio ranging from 0.8 to 1.3 were then produced. Their specific surface areas (SSA, m^2/g) were measured according to Brunauer, Emmett and Teller (BET) protocol (Brunauer et al., 1938) on a Micromeritics Flow-sorb II. Particles diameters were calculated from their SSA values, as $D = 6000/(\rho \times SSA)$, where D (nm) is BET diameter, and $\rho = 3.2\ g\,cm^{-3}$ is the density of SiC. Mass concentration of constitutive element (Si, C) and impurities (O and N) as well as Si/C ratios were deduced from chemical elemental analysis. X-ray powder diffraction showed pure cubic phase (3C-SiC) with the presence of stacking faults (not shown here).

2.2. Nanoparticles dispersion and characterization

Nanoparticles were dispersed in ultrapure sterile water (pH 5.5) by sonication for 30 min at 4 °C, in pulsed mode (1 s on/1 s off), at the concentration of 5 mg/mL (Autotune 750 W, Bioblock Scientific, operated at 28% of amplitude) (Simon-Deckers et al., 2008). These nanoparticle suspensions were then diluted with fetal bovine serum (FBS) (v/v) before being sonicated another 30 min in the same conditions. Nanoparticles diameter were measured by transmission electron microscopy (TEM): a drop of nanoparticles suspension was deposited on a TEM grid, allowed to dry, rinsed, and directly observed with a CM 12 Philips electron microscope operated at 80 kV (CCME Orsay, France). Zeta potentials were measured with a Zetasizer (Malvern Instrument).

Just before cell exposure, suspensions were diluted in cell culture medium, as previously described (Barillet et al., 2010), taking care of adjusting FBS content in all exposure suspensions (total protein content: 1.5–2 g/L). Nanoparticles agglomeration state was thus investigated by photon correlation spectroscopy (PCS) (Malvern Zetasizer).

2.3. Cell culture

A549 human lung carcinoma cells (CCL-185) were purchased from ATCC. Cells were subcultured in DMEM containing 4.5 g/L glucose supplemented with 2 mM L-glutamine, penicillin/streptomycin (50 IU/mL and 50 μg/mL, respectively) and 10% (v/v) FBS. They were maintained at 37 °C in a 5% CO_2/air incubator and passed at confluence.

2.4. Cytotoxicity and intracellular internalization

Cytotoxicity was assessed by using 3-[4,5-dimethylthiazol-2-yl]-2,5-diphenyl tetrazolium bromide (MTT) assay (Mosmann, 1983). Mitochondrial dehydrogenases of viable cells reduce MTT to water-insoluble blue formazan crystals which are then solubilised by dimethyl sulfoxide (DMSO); this assay thus indicates cell mitochondrial activity impairment. Cells were grown to sub-confluence in 96-well plates before being exposed to 100 μL of 1–200 μg/mL of nanoparticles suspensions for 4–48 h (see figure captions for details). After exposure, 10 μL of a 5 mg/mL MTT solution were added to each well. After 1 h at 37 °C, medium was then replaced by 100 μL of DMSO and mixed thoroughly to dissolve the formazan crystals. To limit potential problems due to the possible presence of residual nanoparticles that could interfere with the assay, nanoparticles were allowed to sediment during 1 h and 50 μL of each well were then transferred to another plate. Then, absorbance was measured at 570 nm and cell viability was then determined as a percentage of the negative control (unexposed cells).

Transmission electron microscopic observations were carried out to study nanoparticles internalization into cells. After exposure, cells were fixed with 2.5% glutaraldehyde, post-fixed with OsO_4 and dehydrated in graded concentrations of ethanol (Strum et al., 1971) then embedded in Epon. Ultra-thin sections were cut (80 nm), counterstained with lead citrate and uranyl acetate and observed with a CM 12 Philips electron microscope at 80 kV (CCME Orsay, France).

2.5. Oxidative stress

Oxidative stress was first evaluated through measurements of intracellular reactive oxygen species (ROS) formation. To that purpose, the increasing fluorescence of 2′,7′-dichlorodihydrofluorescein diacetate acetyl ester (H2DCF-DA, Invitrogen) was monitored (Oyama et al., 1994). After exposure to nanoparticles, cells were washed twice with PBS, and incubated 30 min at 37 °C with 80 μM H2DCF-DA, then harvested by scraping. The fluorescence intensity was measured with excitation at 480 nm and emission at 530 nm (Molecular Devices Gemini X fluorescence spectrophotometer) and normalized by protein concentration.

Glutathione concentration was evaluated, *e.g.* total (GSH + GSSG) and reduced glutathione (GSH) contents (Vandeputte et al., 1994). Cells lysates were prepared by scraping in phosphate buffer supplemented with glycerol and phenylmethanesulfonyl fluoride, frozen in liquid nitrogen then thawed at 37 °C three times. They were then centrifuged (4 °C, 15 min, 10,000 × *g*) and supernatants were collected, their protein concentration was measured and normalized. Reduced glutathione (GSH) content was measured via its oxidation by 5,5′-dithiobis(2-nitrobenzoic acid) (DTNB), which leads to the formation of 5-thio(2-nitrobenzoic acid) (TNB), a yellow by-product absorbing at 405 nm. The same protocol was applied for the determination of total glutathione content (GSH + GSSG), with a preliminary step of reduction of oxidized glutathione (GSSG) by glutathione reductase (GR). After addition of DTNB to cell lysates, absorbance at 405 nm was followed during 5 min. GSH and GSH + GSSG concentrations in cell lysates were then determined by comparison to GSH calibration curves.

The activities of enzymes responsible for cellular oxidative status maintenance, glutathione reductase (Carlberg et al., 1985), superoxide dismutase (SOD) (Paoletti et al., 1986), and catalase (CAT) (Beers and Sizer, 1952), were evaluated, also on the cell lysates prepared for GSH measurements. For GR activity measurement, the assay is based on the oxidation of reduced glutathione by DTNB. Phosphate buffer supplemented with 1 mM EDTA, 400 μM DTNB, 300 μM NADPH and 800 μM GSSG was added to the cell lysate. Absorbance at 405 nm was then read continuously during 5 min. Glutathione reductase activity was then calculated from a GR standard calibration curve. SOD activity was measured as an indirect assay in which β-mercaptoethanol competes with endogenous SOD for nicotinamide adenine dinucleotide (NADH) oxidation by $O_2^{\bullet -}$. One unit of SOD activity is defined as the amount that causes 50% inhibition of NADH oxidation under specific conditions. Phosphate buffer supplemented with 350 μM NADH, 3 mM EDTA, and 1.5 mM and $MnCl_2$. 2-mercapto-ethanol (10 mM) was added to cell lysates. After a 20 min incubation period at room temperature, absorbance at 340 nm was read during 5 min. SOD activity was then determined by comparison with a SOD activity calibration curve. Catalase activity was measured by spectrophotometrically monitoring the disappearance of exogenous H_2O_2. Standard solutions of known CAT activities (0.5–50 U/mL) were prepared in phosphate buffer (100 mM, pH 7.8). Hydrogen peroxide was added to cell lysate, then absorbance was read at 240 nm for 5 min. Catalase activity was then deduced to CAT standard calibration curve.

2.6. Genotoxicity

Nanoparticle-induced DNA damage was assessed through the alkaline version of comet assay (Singh et al., 1988). Microscope slides were coated with 1% normal melting point agarose (NMA) and allowed to dry. Around 10,000 cells (75 μL of each cell suspension) were mixed with 1% low melting point agarose (LMPA), deposited over the agarose layer. Then 0.5% LMPA was dispensed on each slide and allowed to solidify on ice. The slides were immersed in cold lysis solution (2.5 M NaCl, 100 mM EDTA, 10 mM Tris, 10% DMSO, 1% Triton X-100) for 1 h at 4 °C. DNA was then allowed to unwind for 30 min in alkaline electrophoresis solution (300 mM NaOH, 1 mM EDTA, pH > 13). Electrophoresis was performed in a field of 0.7 V/cm and 300 mA current for 24 min. Samples were then neutralized with 0.4 M Tris pH 7.5 and stained with 50 μL of 20 μg/mL ethidium bromide. At least 50 comets per slide were analyzed under a fluorescence microscope (Zeiss) equipped with a 350–390 nm excitation and 456 nm emission filter at ×20 magnification. Comet length and intensity were measured by using Comet IV software (Perceptive Instruments, Suffolk, UK).

2.7. Statistical analysis

Each experiment was performed at least three times. Statistical tests were run using the Statistica 7.1 software (Statsoft, Chicago, IL, USA). As normality assumptions for valid parametric analyses, even after data log transformation, were not satisfied (Kolmogorov–Smirnov tests), non-parametric one-way analyses of variance on ranks approach (Kruskal–Wallis) were used. When significance was demonstrated ($p < 0.05$), paired comparisons were run using Mann–Whitney tests.

Table 1
Physico-chemical characteristics of NP-SiC[a].

	SSA (m^2/g)	Size BET (nm)	Size TEM (nm)	Si/C	ζ (mV)	Hydrodynamic diameter (nm)
SiC-A	125	15	17 ± 3	0.8	−24	168 (100%)
SiC-B	134	14	13 ± 3	1.0	−22	125 (100%)
SiC-C	140	13	12 ± 3	1.2	−31	97 (100%)
SiC-D	52	36	31 ± 8	1.1	−28	190 (100%)
SiC-E	33	58	45 ± 18	1.1	−28	280 (100%)

[a] SSA: specific surface area, measured according to Brunauer, Emmett and Teller. Size BET: NP-SiC diameters, calculated from SSA. Size TEM: NP-SiC diameters, measured on transmission electron microscopy (TEM) images. Zeta potential (ζ) was measured just before NP dilution into cell culture medium. Hydrodynamic diameter was measured by PCS after NP dilution into cell culture medium.

3. Results

3.1. Physico-chemical characterization of SiC nanoparticles and suspensions

The five batches of NPs used in this study were produced in our laboratories. As described in Table 1, SiC-A, SiC-B and SiC-C diameters are close, they range from 13 nm to 15 nm. These 3 NPs differ in their Si/C ratio. Si/C ratio of SiC-A is 0.8, meaning that their surface is rather composed of carbon residues. This ratio increases to 1.0 in SiC-B, and to 1.2 in SiC-C, the surface of SiC-C thus contains more Si atoms than the surface of the other SiC-NPs. These Si atoms may oxidize to SiO_2, either spontaneously via interaction with the surrounding atmosphere (air), but also probably during the sonication process (Phely-Bobin et al., 2002). Consequently the surface properties of SiC-A, SiC-B, and SiC-C NPs must differ. The second part of SiC nanoparticles panel is composed of nanoparticles having a constant and high Si/C ratio, 1.1–1.2, and with increasing diameters: SiC-C diameter is 13 nm while SiC-D diameter is 36 nm and SiC-E is 58 nm.

All these nanoparticles are free of metallic impurities, but contain varying amounts of O and N. Their size calculated from their specific surface area is close to their size measured by transmission electron microscopy, meaning that these nanoparticles have a low porosity. TEM images reveal round-shaped nanoparticles, with a narrow size distribution, arranged in a chain-like manner (Fig. 1).

The zeta potential of all these SiC-NPs ranged from −22 mV to −31 mV, these suspensions may thus be considered as electrostatically instable, leading to agglomeration. This assumption was confirmed after dilution in cell culture medium, by the measurement of their hydrodynamic diameter, which reached 100–300 nm. NPs are thus loosely agglomerated when cells are exposed. The diameters of these agglomerates are closely related to the primary diameters of nanoparticles: the bigger a particle, the larger a cluster. Conversely, the hydrodynamic diameter of clusters increased when their Si/C ratio decreased. It is not surprising since the surface of SiC-NPs with high Si/C ratio is presumed to be predominantly made of SiO_2, and consequently more hydrophilic than the surface of SiC nanoparticles with low Si/C ratio, predominantly composed of carbon atoms.

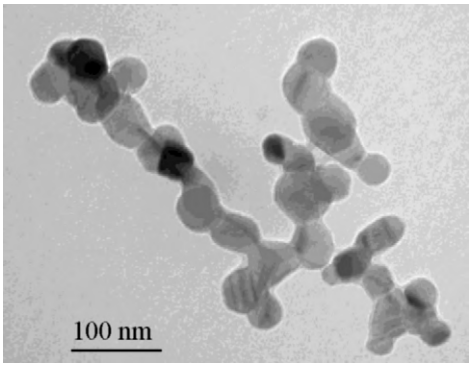

Fig. 1. Size and shape of a cluster of SiC-E NPs. Observation of a drop of dispersed SiC-NP suspension, observed by TEM.

Since NPs suspensions were prepared in fetal bovine serum, their surface may be covered by a layer of proteins. Depending on their hydrophobicity, various proteins may be adsorbed on their surface, leading to a different protein corona. The biological impact of nanoparticles SiC-A, SiC-B and SiC-C would thus depend on the variability of their protein corona, while the biological impact of nanoparticles SiC-C, SiC-D and SiC-E would thus depend on their diameter.

3.2. Cellular uptake and cytotoxicity

Intracellular accumulation of SiC-NPs was investigated by TEM observation of cells exposed to SiC-B for 24 h. NPs were taken up by cells, and were majorly entrapped in various cytoplasmic compartments: either lamellar bodies, specific of surfactant secreting cells such as A549 cells, vacuoles or lysosomes (Fig. 2). In these compartments, they were grouped as clusters of 20–100 nm. NPs were neither detected in mitochondria, nor in endoplasmic reticulum or Golgi. Some NPs were observed in cell nuclei (Fig. 2A), where they were arranged in small clusters (20–30 nm). The overall shape of

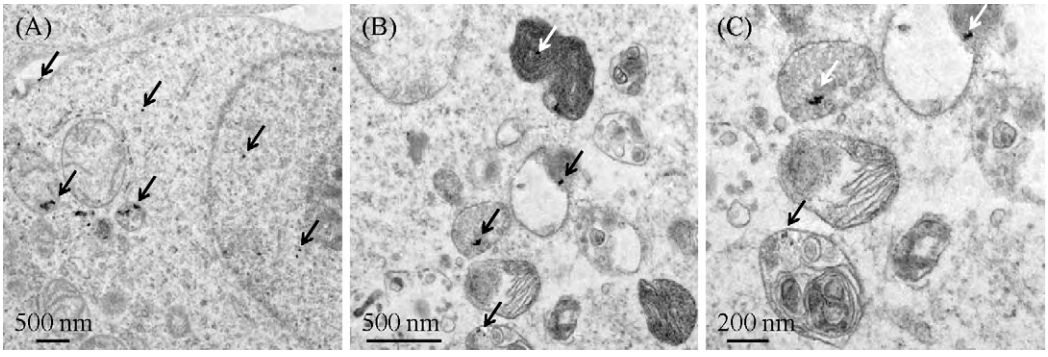

Fig. 2. Intracellular accumulation of SiC-NPs. A549 cells were exposed for 24 h to 50 μg/mL of SiC-B (A, B: bar = 500 nm, C: bar = 200 nm). NPs are indicated by arrows.

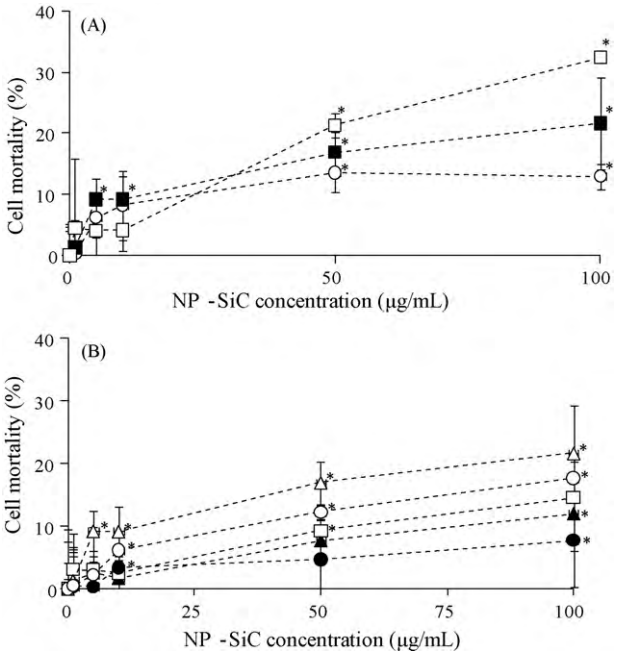

Fig. 3. Cytotoxicity of SiC-NPs in A549 cells. A: typical mortality curves obtained after 4 h (circles), 24 h (black squares), and 48 h (white squares) of exposure to SiC-D. B: mortality curves obtained after 24 h of exposure to SiC-A (black triangles), SiC-B (white squares), SiC-C (black circles), SiC-D (white triangles), SiC-E (white circles). Data are presented as mean ($n = 5–6$) ± SD. Statistical significance $^*p < 0.05$.

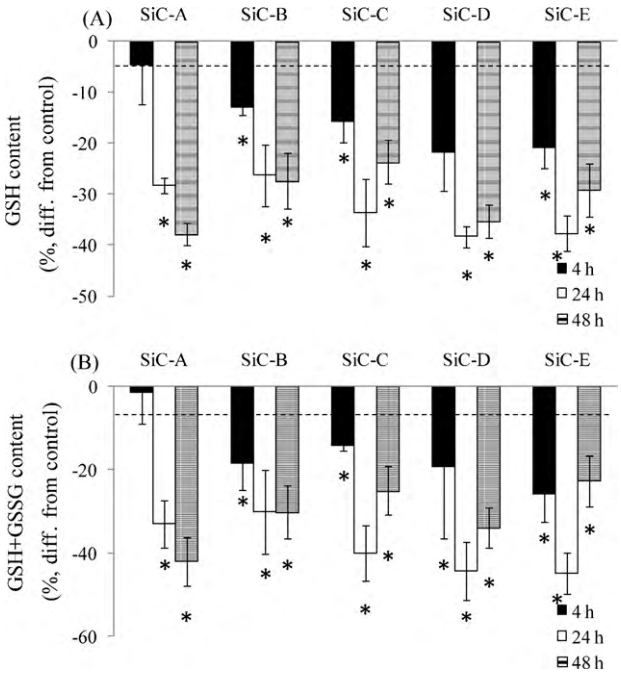

Fig. 5. Effect of SiC-NPs on cellular glutathione content. A549 cells were exposed to 100 μg/mL of SiC-NPs and reduced glutathione (GSH, A) or total glutathione (GSH + GSSG, B) contents were measured. Data are presented as mean percent difference from control ($n = 3$) ± SD. $^*p < 0.05$ versus control (unexposed) cells.

exposed cells was modified as compared to the shape of unexposed cells: exposed cells contained more vesicles and vacuoles in their cytoplasms.

Intracellular accumulation of SiC-NPs induced low but significant cell mortality (Fig. 3). Cell death slightly increased between 4 h and 48 h of exposure (Fig. 3A), and the most drastic condition (48 h, 100 μg/mL, SiC-D) led to 32% of mortality (Fig. 3B). No correlation could be established between cytotoxicity and SiC-NP diameter or Si/C ratio.

3.3. Intracellular ROS production

While SiC-NPs did not cause severe cell mortality, they induced intracellular ROS generation (Fig. 4). ROS production was observed earlier on cells exposed to SiC-B and SiC-C than on cells exposed to SiC-A, suggesting that it depended on Si/C ratio: high Si/C ratio caused earlier intracellular ROS accumulation. ROS accumulation also depended on SiC-NP diameter: it was observed earlier on cells exposed to SiC-C than on cells exposed to SiC-D and SiC-E. Finally, in the conditions that did not led to ROS over-accumulation, *e.g.* exposure to SiC-A, SiC-D and SiC-E for 4 h, intracellular ROS content was significantly lower than in the negative control (unexposed cells).

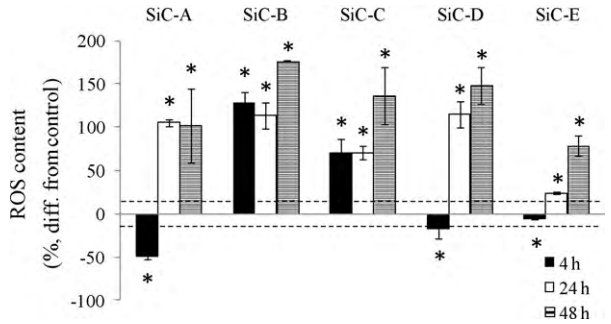

Fig. 4. ROS concentration in cells exposed to SiC-NPs. A549 cells were exposed to 100 μg/mL of SiC-NPs for 4 h, 24 h, or 48 h. Data are presented as mean percent difference from control ($n = 3$) ± SD. $^*p < 0.05$ versus control (unexposed) cells.

3.4. Cellular antioxidant response

Cellular antioxidant response involves the action of intracellular molecular antioxidants such as glutathione, and regulation of antioxidant enzymes activity. First, glutathione content was measured in SiC-NP exposed cells, either in its reduced form (GSH) or as total glutathione content (GSH + GSSG) (Fig. 5). An early consumption of GSH was observed in cells exposed to SiC-NP, whatever their diameter and Si/C ratio. It started after 4 h of exposure, and was further decreased after 24 h and 48 h (Fig. 5A). Total glutathione content (GSH + GSSG) followed the same trend: an early decrease was observed, which was amplified after 24 h and 48 h. The only conditions where GSH and GSH + GSSG were not significantly decreased were exposure to SiC-A, 4 h (GSH and GSH + GSSG) and SiC-D, 4 h (GSH + GSSG only). In these conditions GSH and GSH + GSSG were also reduced, but it was not statistically significant.

The activities of antioxidant enzymes were also modulated (Fig. 6). Glutathione reductase activity was globally decreased, except for cells exposed to SiC-A, SiC-B or SiC-E for 4 h. This decrease occurred early: it was observed after 4 h of exposure, and maintained after 24 h and 48 h of exposure (Fig. 6A). Superoxide dismutase activity was also reduced, but this reduction was only statistically significant after 24 h of exposure, and was maintained after 48 h of exposure (Fig. 6B). Finally, catalase activity appeared to be less affected in cells exposed to NP-SiC (Fig. 6C): it was only increased in four conditions (SiC-A, 4 h and 48 h, SiC-C, 4 h, SiC-E, 4 h), and decreased in another one (SiC-C, 4 h).

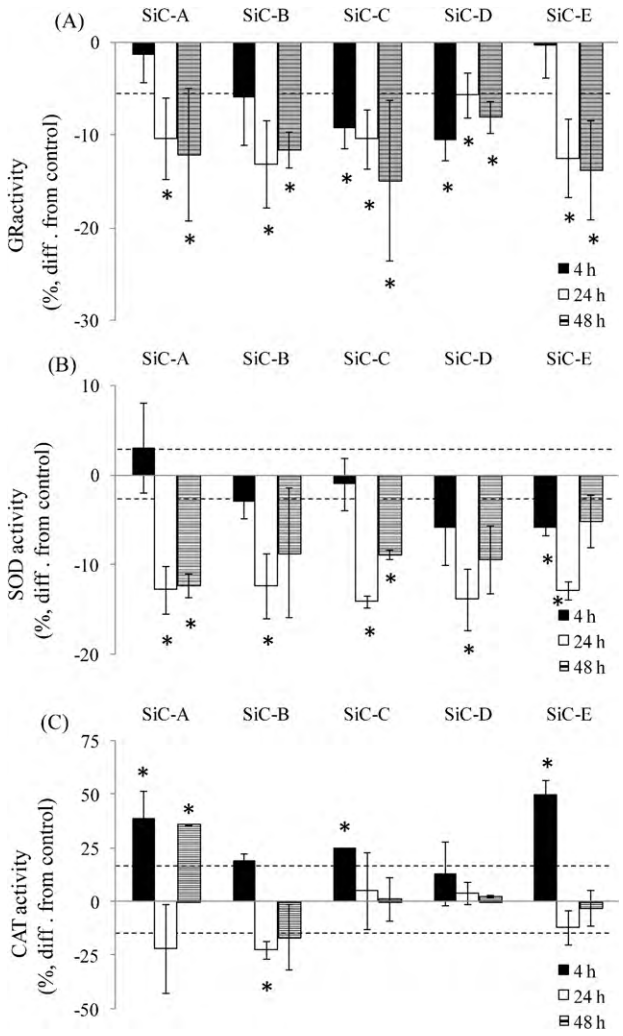

Fig. 6. Effect of SiC-NPs on antioxidant enzymes activities. A549 cells were exposed to 100 μg/mL of SiC-NPs and glutathione reductase (GR, A), superoxide dismutase (SOD, B) and catalase (CAT, C) activities were evaluated. Data are presented as mean percent difference from control ($n = 3$) ± SD. *$p < 0.05$ versus control (unexposed) cells.

3.5. Genotoxicity

Since SiC nanoparticles were observed in cell nuclei and induced modifications in cellular redox status, their impact on DNA integrity was assessed (Fig. 7). The alkaline version of the comet assay was employed; it enables to detect DNA single-, double-strand breaks, and alkali-labile sites. All the tested SiC-NPs induced DNA strand breakages. These lesions were permanently induced in cells exposed to SiC-C, SiC-D, and SiC-E: the comet tail length was increased by 20–30% as compared to unexposed cells whatever the exposure duration (4 h, 24 h or 48 h). Conversely when cells were exposed to SiC-A and SiC-B, the length of comet tails decreased with exposure duration: after 4 h it was 30% longer than in unexposed cells, after 24 h it was 20% (SiC-B) and 3% (SiC-A) of comet length in unexposed cells, and after 48 h it was reduced to 10% (SiC-B) and 3% (SiC-A).

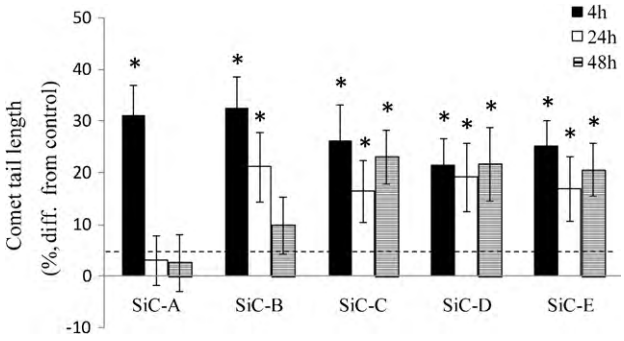

Fig. 7. SiC-NPs impact on DNA integrity. A549 cells were exposed to 50 μg/mL of SiC-NPs for 4 h, 24 h, or 48 h. Comet tail length are presented as mean percent difference from control ($n = 50$) ± SEM. *$p < 0.05$ versus control cells.

4. Discussion

This report demonstrates that SiC-NPs were taken up by A549 cells, where their cytotoxicity was low. Low cytotoxicity of SiC-NPs has already been demonstrated by others authors, working with 4 nm SiC nanocrystals (Fan et al., 2008) or with microscaled SiC particles (Bruch et al., 1993a,b). Fan et al. demonstrated that 4 nm SiC-NPs were accumulated in cells, but that they were highly translocated to cell nuclei (Fan et al., 2008). Conversely, in the present study, only a few SiC-NPs were detected in cell nuclei. This discrepancy can be easily explained since the SiC-NPs used in the present study were much bigger. 4 nm SiC-NPs may reach the nuclear compartment through nuclear pores, whose diameter range between 8 nm and 10 nm. 15–60 nm SiC-NPs may only gain access to nuclei when cells undergo mitosis and their nuclear wall is disrupted. In the cytoplasmic compartment, SiC-NPs are entrapped in vesicles, as in cells exposed to other NPs such as TiO_2-NPs (Simon-Deckers et al., 2008; Stearns et al., 2001). However contrary to TiO_2-NPs, SiC-NPs clusters observed in cytoplasmic vesicles are much smaller. We chose to stabilize SiC-NPs with FBS, which is an efficient dispersant since it may cover SiC-NPs with a protein corona. This protein corona probably induces electrostatic and/or steric repulsion which stabilize NPs in exposure medium. As a consequence small clusters of SiC-NPs may gain access to cell cytoplasm via microdomains, or by caveolae or clathrin-mediated endocytosis, which generate vesicles with diameters smaller than 100 nm (Sahay et al., 2010). On the contrary, TiO_2-NPs are much more agglomerated in cell culture medium, and may rather be internalized in cells by phagocytosis or macropinocytosis. A future study will aim at identifying the protein corona which is formed on the surface of SiC-NPs due to the contact with serum proteins. It must also be noted that serum proteins which are adsorbed on the surface of SiC-NPs may be denaturated by sonication, inducing changes in their conformation and thus in their properties (Gulseren et al., 2007). However these modifications did not induce SiC-NPs agglomeration. Our future study will also evaluate protein conformation modification due to sonication.

SiC-NPs caused major redox disorder in exposed cells: ROS generation, depletion of antioxidant molecules (GSH), and inactivation on antioxidant enzymatic systems (GR and SOD), which are schematically illustrated in Fig. 8. ROS intracellular accumulation may either come from direct ROS production on the surface of NPs, from indirect generation of ROS in cells stressed by NP exposure, or from destabilization of cellular ROS elimination pathways (Li et al., 2008). Metal impurities can also mediate ROS production via Fenton-like and Haber Weiss reactions; however this explanation is excluded since the SiC-NPs used in the present study do not contain any metal-based impurities. Silica NPs are known to directly generate $HO^{\bullet}$ radical in water or in H_2O_2 (Lin et al., 2006). They have also been described as potent stimulator of the respiratory burst in phagocytic cells, leading to the production of $O^{\bullet -}$, H_2O_2, and NO (Fubini and Hubbard, 2003). The sonication process used in the present study to prepare stable suspensions of SiC-NPs, may promote the rapid oxidation of Si surface atoms to SiO_2. The surface

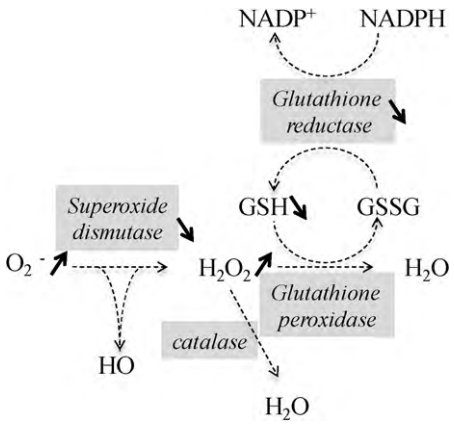

Fig. 8. Schematic representation of cellular redox equilibrium system modulation by SiC-NPs. Modulations of enzyme activities and molecule concentrations are depicted by arrows up (activation or increased concentration) or down (inhibition or decreased concentration).

properties of sonicated SiC-NPs, especially those with a high Si/C ratio, may then be close to the surface properties of silica NPs, and consequently may trigger ROS production on their surface. Carbon black (CB) NPs have also been shown to induce ROS production in acellular medium (Koike and Kobayashi, 2006; Wilson et al., 2002). Since the surface of SiC-NPs with a high Si/C ratio might be oxidized to SiO_2, and the surface of SiC-NPs with a low Si/C ratio is majorly composed of carbon, these phenomena can explain ROS accumulation in SiC-NPs-exposed cells. The exact identification of produced ROS may be different, and more work would be necessary to characterize them. Moreover we show that SiC-NP diameter modulate ROS production. This modulation has also already been described with TiO_2-NPs and CB-NPs, and attributed to higher surface area, and thus higher surface reactivity of the finest NPs (Hussain et al., 2009). We confirm here that this phenomenon can be generalized to SiC-NPs: the finest ones induce a higher ROS production than the bigger ones, certainly due to their higher surface area and thus surface reactivity.

Kinetically, a significant reduction of ROS cellular content was observed in the early exposure time points to SiC-A, SiC-D and SiC-E. ROS may first act as a signal, inducing early activation of cell antioxidant defenses, as described by Feinendegen (2002). Then these antioxidant defenses may be saturated, resulting in ROS intracellular accumulation.

SiC-NPs caused a depletion of cellular GSH, the major molecular antioxidant of cells. GSH may either be released from the cells to the extracellular medium, or be intracellularly oxidized to GSSG by glutathione peroxidase, this reaction being coupled to the reduction of H_2O_2 to H_2O. Since ROS are highly accumulated in SiC-NPs-exposed cells, GSH oxidation to GSSG via glutathione peroxidase is probable. However, total glutathione content (GSH + GSSG) may remain constant, which is not true: GSH + GSSG decreases. Consequently, GSH may be oxidized to GSSG, but GSH and/or GSSG must also be released from cells to the extracellular medium. To support this hypothesis, Brown et al. previously demonstrated that SiC fiber deplete GSH from lung lining fluid (Brown et al., 2000). Moreover Zhang et al. suggested that GSH was released from alveolar macrophages exposed to silica as a consequence of GSH depletion in the extracellular fluid (Zhang et al., 1999). From our result, it can be suspected that SiC-NPs deplete extracellular fluid from GSH and/or GSSG; then cells release these molecules to reestablish glutathione intra/extracellular balance. Moreover GR, responsible for GSSG reduction to GSH, is inactivated. GSH pool is thus not reestablished, leading to accumulation of H_2O_2 in cells. SOD, which is responsible for $O_2^{\bullet -}$ dismutation to H_2O_2, is also partially inactivated in SiC-NPs-exposed cells. This may result in $O_2^{\bullet -}$ intracellular accumulation, which may cause damage to biological molecules.

Results published in the literature concerning genotoxic potential of silica-based and carbon-based nanoparticles are conflicting. These NP have been shown to generate DNA damage (Wang et al., 2007), while others report that they do not exert significant genotoxicity (Barnes et al., 2008; Jin et al., 2007). Here, we show that SiC-NPs cause DNA breakage. The genotoxicity of NP-SiC may come from direct interaction between NP and DNA, since some NPs reach the nuclear compartment. However nuclear accumulation of SiC-NPs is low, DNA damage is thus rather indirectly generated, certainly through the attack of DNA by over-accumulated ROS, which may gain access to cell nucleus by diffusion through nuclear pores and then attack DNA. Genotoxicity appeared to be transient in cells exposed to SiC-A and SiC-B, and permanent in cells exposed to the other NP-SiC. Transient response may be due to the activation of DNA repair systems; this hypothesis is presently under investigation.

Finally, the comparison of cellular responses induced by this panel of SiC-NPs led to the conclusion that SiC-NPs with high Si/C ratio induced ROS production and GR activity inhibition earlier than SiC-NPs with low Si/C ratio. They also induced a more persistent genotoxicity. The presence of SiO_2 residues on the surface of these NPs then renders them more toxic. Secondly, the finest SiC-NPs, with diameters around 15 nm, also cause the earliest ROS production and GR activity inhibition in cells, but had no influence on DNA damage appearance. This confirms the already well documented assumption that small NPs are more toxic than larger ones (Simon-Deckers et al., 2008).

5. Conclusions

Altogether, these results attest that SiC-NPs are accumulated in lung cells, *in vitro*, where they do not cause strong cell mortality, but induce major redox disturbance and DNA damage. These cellular responses both depend on SiC-NP cluster size, and on Si/C ratio. Presently, the links between the observed cellular responses are not clear, and more studies are necessary to further understand the underlying mechanisms. However, considering these data, SiC-NPs biocompatibility may be reconsidered, and these NPs should be manipulated with caution until more toxicological information is available.

Conflict of interest statement

None declared.

Acknowledgments

This work received funding by the French national research agency (ANR), the French agency for sanitary safety of the environment (AFSSET) and the Ile-de-France region in the framework of C'nano IdF. The authors thank D. Jaillard from CCME (Centre Commun de Microscopie Electronique d'Orsay, France) for helping in TEM sample preparation and observations.

References

Akiyama, I., Ogami, A., Oyabu, T., Yamato, H., Morimoto, Y., Tanaka, I., 2007. Pulmonary effects and biopersistence of deposited silicon carbide whisker after 1-year inhalation in rats. Inhal. Toxicol. 19, 141–147.

Barillet, S., Simon-Deckers, A., Herlin-Boime, N., Mayne-L'Hermite, M., Reynaud, C., Cassio, D., Gouget, B., Carrière, M., 2010. Toxicological consequences of TiO2, SiC nanoparticles and multi-walled carbon nanotubes exposure in several mammalian cell types: an in vitro study. J. Nanopart. Res. 12, 61–73.

Barnes, C.A., Elsaesser, A., Arkusz, J., Smok, A., Palus, J., Lesniak, A., Salvati, A., Hanrahan, J.P., Jong, W.H., Dziubaltowska, E., Stepnik, M., Rydzynski, K., McKerr, G.,

Lynch, I., Dawson, K.A., Howard, C.V., 2008. Reproducible comet assay of amorphous silica nanoparticles detects no genotoxicity. Nano Lett. 8, 3069–3074.
Beers, R.F., Sizer, I.W., 1952. A spectrophotometric method for measuring the breakdown of hydrogen peroxide by catalase. J. Biol. Chem. 195, 133–140.
Bouclé, J., Herlin-Boime, N., Kassiba, A., 2005. Influence of silicon and carbon excesses on the aqueous dispersion of SiC nanocrystals for optical application. J. Nanopart. Res. 7, 275–285.
Brown, D.M., Beswick, P.H., Bell, K.S., Donaldson, K., 2000. Depletion of glutathione and ascorbate in lung lining fluid by respirable fibres. Ann. Occup. Hyg. 44, 101–108.
Bruch, J., Rehn, B., Song, H., Gono, E., Malkusch, W., 1993a. Toxicological investigations on silicon carbide. 1. Inhalation studies. Br. J. Ind. Med. 50, 797–806.
Bruch, J., Rehn, B., Song, W., Gono, E., Malkusch, W., 1993b. Toxicological investigations on silicon carbide. 2. In vitro cell tests and long term injection tests. Br. J. Ind. Med. 50, 807–813.
Brunauer, S., Emmett, P.H., Teller, E., 1938. Adsorption of gases in multimolecular layers. J. Am. Chem. Soc. 60, 309–319.
Carlberg, I., Mannervik, B., Alton, M., 1985. Glutathione reductase. Methods in Enzymology, vol. 113. Academic Press, pp. 484–490.
Cullen, R.T., Miller, B.G., Davis, J.M., Brown, D.M., Donaldson, K., 1997. Short-term inhalation and in vitro tests as predictors of fiber pathogenicity. Environ. Health Perspect. 105 (Suppl. 5), 1235–1240.
Fan, J., Li, H., Jiang, J., So, L.K., Lam, Y.W., Chu, P.K., 2008. 3C-SiC nanocrystals as fluorescent biological labels. Small 4, 1058–1062.
Feinendegen, L.E., 2002. Reactive oxygen species in cell responses to toxic agents. Hum. Exp. Toxicol. 21, 85–90.
Fubini, B., Hubbard, A., 2003. Reactive oxygen species (ROS) and reactive nitrogen species (RNS) generation by silica in inflammation and fibrosis. Free Radic. Biol. Med. 34, 1507–1516.
Gulseren, I., Guzey, D., Bruce, B.D., Weiss, J., 2007. Structural and functional changes in ultrasonicated bovine serum albumin solutions. Ultrason. Sonochem. 14, 173–183.
Herlin-Boime, N., Vicens, J., Dufour, C., Ténégal, F., Reynaud, C., Rizk, R., 2004. Flame temperature effect on the structure of SiC nanoparticles grown by laser pyrolysis. J. Nanopart. Res. 6, 63–70.
Hussain, S., Boland, S., Baeza-Squiban, A., Hamel, R., Thomassen, L.C., Martens, J.A., Billon-Galland, M.A., Fleury-Feith, J., Moisan, F., Pairon, J.C., Marano, F., 2009. Oxidative stress and proinflammatory effects of carbon black and titanium dioxide nanoparticles: role of particle surface area and internalized amount. Toxicology 260, 142–149.
Jin, Y., Kannan, S., Wu, M., Zhao, J.X., 2007. Toxicity of luminescent silica nanoparticles to living cells. Chem. Res. Toxicol. 20, 1126–1133.
Koike, E., Kobayashi, T., 2006. Chemical and biological oxidative effects of carbon black nanoparticles. Chemosphere 65, 946–951.
Lapin, C.A., Craig, D.K., Valerio, M.G., McCandless, J.B., Bogoroch, R., 1991. A subchronic inhalation toxicity study in rats exposed to silicon carbide whiskers. Fundam. Appl. Toxicol. 16, 128–146.
Lewinski, N., Colvin, V., Drezek, R., 2008. Cytotoxicity of nanoparticles. Small 4, 26–49.
Li, N., Xia, T., Nel, A.E., 2008. The role of oxidative stress in ambient particulate matter-induced lung diseases and its implications in the toxicity of engineered nanoparticles. Free Radic. Biol. Med. 44, 1689–1699.
Lin, W., Huang, Y.W., Zhou, X.D., Ma, Y., 2006. In vitro toxicity of silica nanoparticles in human lung cancer cells. Toxicol. Appl. Pharmacol. 217, 252–259.
Melinon, P., Masenelli, B., Tournus, F., Perez, A., 2007. Playing with carbon and silicon at the nanoscale. Nat. Mater. 6, 479–490.
Mosmann, T., 1983. Rapid colorimetric assay for cellular growth and survival: application to proliferation and cytotoxicity assays. J. Immunol. Methods 65, 55–63.
Oyama, Y., Hayashi, A., Ueha, T., Maekawa, K., 1994. Characterization of 2′,7′-dichlorofluorescin fluorescence in dissociated mammalian brain neurons: estimation on intracellular content of hydrogen peroxide. Brain Res. 635, 113–117.
Paoletti, F., Aldinucci, D., Mocali, A., Caparrini, A., 1986. A sensitive spectrophotometric method for the determination of superoxide dismutase activity in tissue extracts. Anal. Biochem. 154, 536–541.
Phely-Bobin, T., Chattopadhyay, D., Papadimitrakopoulos, F., 2002. Characterization of mechanically attrited Si/SiOx nanoparticles and their self-assembled composite films. Chem. Mater. 14, 1030–1036.
Rodelsperger, K., Bruckel, B., 2006. The carcinogenicity of WHO fibers of silicon carbide: SiC whiskers compared to cleavage fragments of granular SiC. Inhal. Toxicol. 18, 623–631.
Sahay, G., Alakhova, D.Y., Kabanov, A.V., 2010. Endocytosis of nanomedicines. J. Controlled Release 145 (3), 182–195.
Simon-Deckers, A., Gouget, B., Mayne-L'hermite, M., Herlin-Boime, N., Reynaud, C., Carriere, M., 2008. In vitro investigation of oxide nanoparticle and carbon nanotube toxicity and intracellular accumulation in A549 human pneumocytes. Toxicology 253, 137–146.
Singh, N.P., McCoy, M.T., Tice, R.R., Schneider, E.L., 1988. A simple technique for quantitation of low levels of DNA damage in individual cells. Exp. Cell Res. 175, 184–191.
Stearns, R.C., Paulauskis, J.D., Godleski, J.J., 2001. Endocytosis of ultrafine particles by A549 cells. Am. J. Respir. Cell Mol. Biol. 24, 108–115.
Strum, J.M., Wicken, J., Stanbury, J.R., Karnovsky, M.J., 1971. Appearance and function of endogenous peroxidase in fetal rat thyroid. J. Cell Biol. 51, 162–175.
Svensson, I., Artursson, E., Leanderson, P., Berglind, R., Lindgren, F., 1997. Toxicity in vitro of some silicon carbides and silicon nitrides: whiskers and powders. Am. J. Ind. Med. 31, 335–343.
Vandeputte, C., Guizon, I., Genestie-Denis, I., Vannier, B., Lorenzon, G., 1994. A microtiter plate assay for total glutathione and glutathione disulfide contents in cultured/isolated cells: performance study of a new miniaturized protocol. Cell Biol. Toxicol. 10, 415–421.
Vaughan, G.L., Jordan, J., Karr, S., 1991. The toxicity, in vitro, of silicon carbide whiskers. Environ. Res. 56, 57–67.
Vaughan, G.L., Trently, S.A., Wilson, R.B., 1993. Pulmonary response, in vivo, to silicon carbide whiskers. Environ. Res. 63, 191–201.
Wang, J.J., Sanderson, B.J., Wang, H., 2007. Cytotoxicity and genotoxicity of ultrafine crystalline SiO_2 particulate in cultured human lymphoblastoid cells. Environ. Mol. Mutagen. 48, 151–157.
Wilson, M.R., Lightbody, J.H., Donaldson, K., Sales, J., Stone, V., 2002. Interactions between ultrafine particles and transition metals in vivo and in vitro. Toxicol. Appl. Pharmacol. 184, 172–179.
Zhang, Z., Shen, H.M., Zhang, Q.F., Ong, C.N., 1999. Critical role of GSH in silica-induced oxidative stress, cytotoxicity, and genotoxicity in alveolar macrophages. Am. J. Physiol. 277, L743–748.